Excitation of San Andreas tremors by thermal instabilities below the seismogenic zone

Lifeng Wang and Sylvain Barbot January 2020

Abstract

The relative motion of tectonic plates is accommodated at boundary faults through slow and fast ruptures that encompass a wide range of source properties. Near the Parkfield segment of the San Andreas fault, deep low-frequency earthquakes and slow-slip events take place deeper than most seismicity, at temperature conditions typically associated with stable sliding. However, laboratory experiments indicate that the strength of granitic gouge decreases with increasing temperature above 350°C, providing a possible mechanism for weakening if temperature is to vary dynamically. Here, we argue that recurring low-frequency earthquakes and slow-slip transients at these depths may arise due to shear heating and the temperature dependence of frictional resistance. Recurring thermal instabilities can explain the recurrence pattern of the mid-crustal low-frequency earthquakes and their correlative slip distribution. Shear heating associated with slow slip is sufficient to generate pseudotachylyte veins in host rocks even when fault slip is dominantly assismic.

Introduction

Recent seismo-geodetic observations have illuminated episodic deformation at the root of active strike-slip faults and megathrusts alike around the world, revealing a wide variety of slip events that fill the spectrum between slow and fast slip [1]. Tremor emissions below the seismogenic zone are often associated with slow slip [2], but the underlying physics remains elusive. Several mechanisms have been proposed to explain the slow-slip phenomenon, including large nucleation size [3], dilatant strengthening [4], and semi-brittle creep [5], but the important role of fluids is often invoked [6]. The simultaneous tremor or low-frequency earthquake (LFE) emissions are thought to represent a form of deterministic chaos emerging from the nonlinear dynamics [7] or the response of a multi-scale rock assembly [8].

Swarms of LFE can be found on the San Andreas fault near the Parkfield segment [9], occupying a separate depth interval in the crust from regular seismicity (Figure 1), presenting along-strike variations in recurrence patterns, amplitude, and sensitivity to tidal stress [10]. The shallowest source of mid-crustal LFE, northwest of Parkfield, that recurs frequently, every 1 to 15 months, clustering seismic events for days to weeks at a time, has been clearly associated with slow-slip transients based on geodetic data [11]. These observations challenge our fundamental assumptions about the rheology of the continental crust. Although the down-dip segmentation of rupture style is widespread at active faults [12], these seismic emissions take place at depths typically associated with stable creep in a continental setting, preventing stress accumulation and the development of frictional instabilities.

Rapid slip below the seismogenic zone has been found in different seismic settings [13, 14], often explained in a top-down model where seismic activity in the upper drives afterslip and aftershocks at greater depth. In contrast, we argue that the coupling between shear heating and the temperature dependence of frictional resistance and contact healing may be responsible for the development of slow-slip events in the velocity-strengthening domain below the seismogenic zone. Laboratory experiments

on granitic and quartz-rich gouge under high pore-fluid pressure [15, 16] indicate velocity-weakening and temperature-strengthening friction between about 50° and 350°C, explaining the location of the seismogenic zone [17]. The same set of experiments also indicates simultaneous velocity-strengthening and temperature-weakening behavior below the seismogenic zone, at ambient temperatures above 350°C. As temperature may vary dramatically with shear heating [18, 19], the temperature-weakening behavior of steady-state friction may offer the conditions for episodic slip.

To support these claims, we first describe a constitutive framework for rate-, state-, and temperature-dependent friction, highlighting the necessary condition for the emergence of thermal instabilities with velocity-strengthening behavior. We then describe the emergence of slow-slip events in a simplified spring-slider system in non-isothermal condition. Finally, we explain the recurrence pattern and the correlative slip distribution of the shallow LFE sources using three-dimensional simulations. Once tuned to seismogeodetic observations, the model allows us to discuss the dynamic range of temperature during the seismic cycle and its implications for fault fabric in the middle crust, below the seismogenic zone.

Thermally activated constitutive law for fault slip

We simulate the coupled evolution of slip and temperature along the San Andreas fault using a microphysical model of rate-, state-, and temperature-dependent friction based on the evolution of the real area of contact [20], whereby the frictional resistance takes the form

$$\tau = \mu_0 \bar{\sigma} \left(\frac{V}{V_0} \right)^{\frac{a}{\mu_0}} \left(\frac{\theta V_0}{L} \right)^{\frac{b}{\mu_0}} \exp \left[\frac{a}{\mu_0} \frac{Q}{R} \left(\frac{1}{T} - \frac{1}{T_0} \right) \right] , \tag{1}$$

where τ and $\bar{\sigma}$ are the shear and effective normal stress on the fault; V and θ are slip velocity and age of asperity contact, respectively; μ_0 , V_0 , and T_0 are reference friction coefficient, velocity, and temperature, respectively; $a \ll 1$ and $b \ll 1$ are power exponents; and Q is an activation energy for the direct effect of temperature. The age of contact is treated as a state variable with the thermally activated evolution law

$$\dot{\theta} = \exp\left[-\frac{H}{R}\left(\frac{1}{T} - \frac{1}{T_0}\right)\right] - \frac{V\theta}{L} \,, \tag{2}$$

where L is a characteristic weakening distance over which the system evolves towards steady-state and H is the activation enthalpy for contact healing. An increase in temperature leads to an immediate reduction in frictional strength called the direct effect, but also an acceleration of healing and time-dependent strengthening, leading to a competition between the two opposing effects on steady-state strength [15]. In isothermal condition with $T = T_0$, equations (1) and (2) reduce to the multiplicative form of rate-and-state friction [20] with the aging law [21].

Temperature is allowed to vary dynamically due to shear heating and heat diffusion. We consider that deformation occurs in an active shear zone with a $\sim 1\,\mathrm{m}$ thick fault core made of several sub-parallel, partially overlapping primary slip surfaces that localize slip over a $\sim 1\,\mathrm{mm}$ -thick active shear layer. The localization of fault slip during any single slip event makes shear heating efficient, even though the overall shear zone may be quite large when considering all the primary and secondary slip surfaces left behind from previous events. As the primary and secondary slip surfaces may overlap partially, the temperature gradient is lower within the fault core than outside of it and temperature diffusion within the fault core is inefficient. In contrast, because of their high fracture density, the damaged rocks outside the fault core often have a high fault-perpendicular permeability and they may advect heat away from the fault effectively [22]. In addition, because of the widely different length scales involved, thermal diffusion in the fault-parallel direction can be neglected. To keep the problem tractable, we may approximate this structural setting by considering a membrane diffusion where fault temperature can be treated as another state variable with the evolution law

$$\dot{T} = -\frac{D}{W^2} \left(T - T_b \right) + \frac{\tau V}{w \rho c} \,, \tag{3}$$

where T is the temperature in the shear zone, D is the average thermal diffusivity in the surrounding damage zone of thickness W, the product ρc is the specific heat per unit volume in the fault zone, T_b is the bath temperature outside the fault zone, which is considered in drained, isothermal condition, and w is the thickness of the active shear layer (Figure 2). We neglect the evolution of pore pressure on the fault and its effect on strength. Equations (1), (2), and (3) form a complete constitutive framework for the evolution of friction and fault slip. The dynamics of the system is eventually controlled by the spatial distribution of the thermo-mechanical properties and the mechanisms of stress distribution [7].

Slow-slip events as thermal instabilities

We first explore the range of physical conditions for the emergence of slow-slip events with duration of weeks and recurrence times of the order of one year using a spring-slider assembly controlled by equations (1), (2), and (3). The emergence of frictional instabilities is conditioned on the rate- and temperature-dependence of friction at steady-state [15, 21]. Velocity-weakening occurs for a - b < 0 and temperature-strengthening for aQ - bH < 0. To explain the seismic emission below the seismogenic zone consistent with laboratory data on granitic rocks and quartz gouge, we focus on a velocity-strengthening (a - b > 0), but temperature-weakening (aQ - bH > 0) fault patch embedded in a rock matrix at temperature $T_b = 400$ °C, representative of mid-crustal conditions with a 20°C/km geothermal gradient. Slow-slip events emerge for a wide range of thermo-mechanical parameters, but we present a case where the peak temperature throughout the seismic cycle remains below the liquidus of wet granite, between 900 and 1100°C depending on composition. The physical parameters are summarized in Table S1.

Away from initial conditions, when the system is loaded at a constant rate, the mechanical system oscillates in closed orbits formed by any pair among velocity, friction, age of contact, and temperature, in repeating cycles (Figure 2). The system traverses six stages with distinct velocity, temperature, or stress patterns. A long nucleation initiates at stage 1, when stress accumulates, but diffusion continues to dominate the temperature evolution. At the onset of stage 2, shear stress is sufficient for shear heating to overcome diffusion and for temperature to start increasing. At stage 3, temperature-weakening accelerates fault slip, leading to a peak in slip velocity when steady state is reached. At this point, temperature is high enough to make healing dominate the state evolution, which strengthens the contact and reduces slip velocity. A peak in temperature is reached at the end of stage 4. At the onset of stage 5, shear stress is low enough for diffusion to dominate the temperature evolution. The transition between stages 4 and 5 is a temperature inflection point. During stage 6, the temperature returns to background levels, the fault re-locks, and the stress starts slowly accruing again. As velocity and temperature co-vary, temperature is often out of phase, with, for example, delayed cooling relative to slip deceleration. These stages unfold in a strictly periodic manner due to the absence of any rheological contrast. The mechanical response of a spring-slider assembly with temperature-weakening, velocity-strengthening friction contrasts with the case of isothermal, velocity-weakening friction as the accelerated healing and re-strengthening associated with high temperature in the former allows repeat cycles of slow-slip events without oversized radiation damping.

This simple model demonstrates how the influence of temperature on contact healing and the strength of frictional sliding may govern the nucleation, propagation, and arrest of deep slow-slip events. More complexity in recurrence times, moment, and duration emerges from more sophisticated, three-dimensional simulations.

Deep slow-slip events on the San Andreas fault

Building upon insights from a simple model, we now simulate the deep slow-slip events along the San Andreas fault on a planar, finite fault embedded in an elastic half-space using the boundary integral method [7, 23]. We use the radiation-damping approximation [24], as neglecting the wave-mediated stress transfer is appropriate in the slow-slip regime.

We consider a rectangular domain from 10 to 26 km depth extending from 12 to 58 km northwest of Parkfield with velocity-strengthening, temperature-weakening properties throughout (Figure 3). The

thermo-mechanical properties are uniform, except for the thickness of the active shear layer and the background temperature. We assign a narrow active shear zone thickness of 0.14 mm in a rectangular patch centered around the shallowest LFE sources to promote unstable behavior and the development of thermal instabilities in this region (Figure 3). The adopted shear layer thickness is on the low range of field observations [25]. Outside the unstable region, we use a much larger value to promote stability. For the background temperature, we use a thermal gradient of 21°C/km with a surface temperature of 15°C. The physical parameters are summarized in Table S2. A low effective normal stress $\bar{\sigma} = 20 \,\mathrm{MPa}$ is required to reproduce the duration and recurrence times of the LFE bursts, indicating near-lithostatic pore fluid pressure. In general, low normal stress hinders efficient shear heating, but this is compensated for in the narrow unstable region by a thin active shear zone. We simulate the dynamics of fault slip on the deep San Andreas fault for a period of 300 years and focus on a representative decade that showcases a wide range of rupture sizes. The long simulation time allows us to examine the long-term space-time clustering of slow-slip events and to mitigate the possible bias from initial conditions.

We obtain a complex sequence of slow-slip events associated with spontaneously emerging thermal instabilities. Large variations of cumulative slip distributions can be found among slow-slip events, as rupture may sometimes propagate far into the surrounding stable region due to the smooth transition from slow slip to afterslip and then re-locking near the source region (Figure 3). Simulation of surface displacements at GPS stations during the seismic cycle indicates a weak contribution from the slow-slip events, accounting to less than 1 mm in a decade, explaining the challenge posed by their geodetic detection [11]. The coupled evolution of slip, stress, and temperature during the seismic cycle (Figure 4) show some remarkable differences with the simpler spring-slider model, as more complexity in recurrence patterns can take place in a three-dimensional model. The sequence of slow-slip events is aperiodic with full and partial ruptures of varying sizes of the unstable patch. The slip per event averages 30 microns distributed over 3 km leading to stress drops of the order of 1 kPa, small enough for the slow-slip cycle to be perturbed by tidal stresses, which are of the order of 0.1 and 4 kPa for the shear and normal components, respectively [26].

The numerical simulation generates a large catalogue of moment-magnitude (Mw) 2.4 to 4.72 events, with a concentration of events with Mw ~ 4.5 (Figure 5), in accordance with the average magnitude of geodetically determined events [11]. However, the model suggests a wide range of event sizes due to the elongated shape of the unstable region. The simulated slow-slip events recur every few weeks to about 20 months, most frequently between 1 and 4 months, with a duration between 1 and 5 weeks, most events propagating for 1 to 3 weeks, sharing the characteristics of the bursts of LFE (Figure 5a,b). The moment-duration relationship of the simulated events occupy a wide space delineated by linear and cubic scaling (Figure 5c), compatible with various assessments of moment-duration scaling of natural slow-slip events in other tectonic settings [27, 28]. However, the moment-duration scaling differs for slow and fast events, implying different source properties linked with slip velocity and shear heating.

The concordance of the model with various seismo-geodetic constraints on the recurrence of LFE swarms and the underlying slow-slip events gives us confidence to discuss other predictions of the model that cannot be directly assessed based on geophysical data. The evolution of temperature in the unstable temperature-weakening region (Figure 4) reveals that shear heating during slow-slip events may increase the temperature on the fault by hundreds of degrees, systematically exceeding the solidus of wet granite, i.e., about 600° C at 20 km depth, yet rarely reaching the wet liquidus, around $900\text{-}1100^{\circ}$ C. The distribution of temperature is highly heterogeneous, with the highest temperatures only attained at the center of the slip distributions, where both slip and slip velocity reach their local maximum. During these week-long pulses of high temperature, the maximum velocity attains only about 10^{-7} m/s , far below the seismic regime.

Discussion

Our results indicate that partial melting may occur around faults due to shear heating, even though the deformation is mostly aseismic, characterized by peak slip velocities only hundred times higher that the tectonic rate (about 1 nm/s), yet much lower than in the seismic regime (about 1 m/s). These inferences

are compatible with observations of pseudotachylytes vein injections [29] and cockade structures [30, 31] at exhumed fault zones that associate the presence of hot fluids or melts with rapid, localized deformation. However, our results suggests that these and other high-temperature proxies [29] may be compatible with the slow-slip regime, reconciling similar observations from laboratory experiments on granitoid cataclasites [32].

Our model does not explicitly resolve the seismic emissions, which operate at smaller length scales and shorter time scales. However, given the near-liquidus temperatures reached at some locations, fast slip may be caused by flash weakening associated with partial melting at isolated hotspots. Laboratory experiments at high slip speed indicate that strong weakening may be associated with lubrication of the fault surface by partial melting [33], gouge amorphization [34], or by pressurization of pore fluids [e.g., 35], all thermally activated phenomena associated with shear heating. Considering the probable presence of pseudotachylytes, we speculate that flash weakening may be activated during the Parkfield slow-slip events at the locations where near-liquidus temperatures are reached, despite the overall low slip velocity. These partial melt pockets may populate the fault at various locations during the seismic cycle following the stress shadows from previous ruptures, or be associated with heterogeneity enhancing local shear heating, such as increased normal stress or a thinner active shear zone. Since the regions reaching the highest temperatures represent a small fraction of the slip distribution of any slow-slip event, this may explain the dominance of aseismic deformation in the cumulative moment of slow slip.

Spontaneously occurring deformation in the mid-crust potentially associated with partial melting argues against a top-down control on crustal dynamics [13]. Instead, the positive feedback between shear heating and temperature-weakening friction provides a mechanism for the spontaneous development of thermal instabilities in the middle crust, even outside any perturbation from the seismic cycle in the seismogenic zone. The complexity of slow-slip event recurrence patterns associated with full and partial ruptures of the temperature-weakening region exemplifies how transient slow slip may redistribute stress and trigger LFE at various times and places, providing an explanatory context for the along-strike variation of LFE activity along the San Andreas fault. Indeed, if creep is accelerated by weakening processes, the creep-mediated stress transfer may operate efficiently at larger distances than with static or wave-mediated stress transfer.

The collective seismological and geodetic observations at the Parkfield segment of the San Andreas fault illuminate a cohesive picture of the fault zone behavior in the brittle layer (Figure 6). Considering the velocity-dependence of frictional resistance helps define the extent of the seismogenic zone, presumably associated with a narrow cataclasite interface [16]. Below the seismogenic zone, the fault fabric may consist in a thicker active shear layer made of a distributed network of primary slip surfaces within a fault core. In this active shear zone, the frictional resistance decreases with more elevated temperature and frictional instabilities may develop, depending on the internal configuration of the shear zone, which affects the stability condition. The shear zone may become mylonitic at greater depths, below the brittle-ductile transition.

Thermal instabilities represent a robust interpretation for the slow-slip events in the continental crust, below the seismogenic zone, because the temperature-weakening properties of quartzo-feldspathic rocks at these conditions are well constrained from laboratory experiments. Thermal instabilities may occur in other tectonic settings as simultaneous velocity-strengthening, temperature-weakening friction has been inferred for carbonate [36], phyllosilicate [37, 38], calcite [39] and serpentinite gouges in various hydrothermal conditions. However, slow slip instabilities below the seismogenic zone at subduction zones may be caused by different processes due to the velocity-weakening, temperature-strengthening friction of serpentinite [40] in these conditions and the predominance of fluid circulation.

While the velocity-weakening and temperature-strengthening properties of granitic rocks at low temperature, hydrous conditions are important to define the boundaries of the seismogenic zone, the velocity-strengthening and temperature-weakening properties of quartzo-feldspathic rocks in shear zones at more elevated temperatures may play an important role on the strength of the mid-crust in the brittle regime and for the rapid redistribution of stress through slow-slip events and slow earthquakes below the seismogenic zone.

Acknowledgements

We appreciate the constructive comments from three anonymous reviewers. LW is supported by the National Natural Science Foundation of China under grant number NSFC-41674067 and NSFC-U1839211. SB is supported in part by the National Science Foundation under award number EAR-1848192.

Author contributions

S.B. designed the study. L.W and S.B conducted the study and wrote the manuscript.

Competing interests

There are no competing interests.

Data and materials availability

All data needed to evaluate the conclusions in the paper are present in the paper. All additional data related to this paper may be requested from the authors.

References

- [1] Kazushige Obara. Nonvolcanic deep tremor associated with subduction in southwest japan. *Science*, 296(5573):1679–1681, 2002.
- [2] G. Rogers and H. Dragert. Episodic tremor and slip on the Cascadia subduction zone: The chatter of silent slip. *Science*, 300(5627), June 2003.
- [3] DM. Veedu and S. Barbot. The Parkfield tremors reveal slow and fast ruptures on the same asperity. *Nature*, 532(7599):361–365, 2016.
- [4] P. Segall, A. M. Rubin, A. M. Bradley, and J. R. Rice. Dilatant strengthening as a mechanism for slow slip events. *J. Geophys. Res.*, 115(B12305), 2010.
- [5] A. Goswami and S. Barbot. Slow-slip events in semi-brittle serpentinite fault zones. *Scientific reports*, 8(1):6181, 2018.
- [6] Pascal Audet and Andrew J Schaeffer. Fluid pressure and shear zone development over the locked to slow slip region in Cascadia. *Science advances*, 4(3):eaar2982, 2018.
- [7] S. Barbot. Slow-slip, slow earthquakes, period-two cycles, full and partial ruptures, and deterministic chaos in a single asperity fault. *Tectonophysics*, 2019.
- [8] Å Fagereng and R. H. Sibson. Mélange rheology and seismic style. Geology, 38(8):751–754, 2010.
- [9] D. R. Shelly. Migrating tremors illuminate complex deformation beneath the seismogenic San Andreas Fault. *Nature*, 463:648–652, 2010.
- [10] Amanda M Thomas, Robert M Nadeau, and Roland Bürgmann. Tremor-tide correlations and nearlithostatic pore pressure on the deep San Andreas fault. Nature, 462(7276):1048–1051, 2009.
- [11] B. Rousset, R. Bürgmann, and M. Campillo. Slow slip events in the roots of the san andreas fault. Science Advances, 5(2):eaav3274, 2019.
- [12] Kazushige Obara and Aitaro Kato. Connecting slow earthquakes to huge earthquakes. *Science*, 353(6296):253–257, 2016.
- [13] B. Jamtveit, Y. Ben-Zion, F. Renard, and H. Austrheim. Earthquake-induced transformation of the lower crust. *Nature*, 556(7702):487–491, 2018.
- [14] Arianne Petley-Ragan, Yehuda Ben-Zion, Håkon Austrheim, Benoit Ildefonse, François Renard, and Bjørn Jamtveit. Dynamic earthquake rupture in the lower crust. Science Advances, 5(7):eaaw0913, 2019.
- [15] F. M. Chester. Effects of temperature on friction: Constitutive equations and experiments with fault gouge. J. Geophys. Res., 99(B4):7247–7261, 1994.
- [16] M. L. Blanpied, D. A. Lockner, and J. D. Byerlee. Frictional slip of granite at hydrothermal conditions. J. Geophys. Res., 100(B7):13045–13064, 1995.
- [17] C. H. Scholz. Earthquakes and friction laws. Nature, 391:37–42, January 1998.
- [18] Robert C Viesca and Dmitry I Garagash. Ubiquitous weakening of faults due to thermal pressurization. Nature Geoscience, 8(11):875, 2015.
- [19] M. S Tarling, S. AF Smith, C. Viti, and J. M Scott. Dynamic earthquake rupture preserved in a creeping serpentinite shear zone. *Nature communications*, 9(1):3552, 2018.
- [20] S. Barbot. Modulation of fault strength during the seismic cycle by grain-size evolution around contact junctions. *Tectonophysics*, 765:129–145, 2019.

- [21] A. Ruina. Slip instability and state variable friction laws. J. Geophys. Res., 88:10,359–10,370, 1983.
- [22] J. R. Rice. Heating and weakening of faults during earthquake slip. J. Geophys. Res., 111:B05311, 2006.
- [23] Q. Qiu, E. M Hill, S. Barbot, J. Hubbard, W. Feng, E. O Lindsey, L. Feng, K. Dai, S. V Samsonov, and P. Tapponnier. The mechanism of partial rupture of a locked megathrust: The role of fault morphology. *Geology*, 44(10):875–878, 2016.
- [24] J. R. Rice, N. Lapusta, and K. Ranjith. Rate and state dependent friction and the stability of sliding between elastically deformable solids. J. Mech. Phys. Solids, 49:1865–1898, 2001.
- [25] Christie D Rowe, Catherine Ross, Mark T Swanson, Stephen Pollock, Nils R Backeberg, Naomi A Barshi, Charlotte E Bate, Samantha Carruthers, Sophie Coulson, Kelian Dascher-Cousineau, et al. Geometric complexity of earthquake rupture surfaces preserved in pseudotachylyte networks. J. Geophys. Res., 123(9):7998–8015, 2018.
- [26] AM Thomas, R Bürgmann, DR Shelly, NM Beeler, and ML Rudolph. Tidal triggering of low frequency earthquakes near Parkfield, California: Implications for fault mechanics within the brittleductile transition. J. Geophys. Res., 117(B5), 2012.
- [27] H. Gao, D. A Schmidt, and R. J Weldon. Scaling relationships of source parameters for slow slip events. *Bull. Seism. Soc. Am.*, 102(1):352–360, 2012.
- [28] S Michel, Adriano Gualandi, and Jean-Philippe Avouac. Similar scaling laws for earthquakes and cascadia slow-slip events. *Nature*, 574(7779):522–526, 2019.
- [29] C. D Rowe and W A Griffith. Do faults preserve a record of seismic slip: A second opinion. J. Structural Geology, 78:1–26, 2015.
- [30] A. Berger and M. Herwegh. Cockade structures as a paleo-earthquake proxy in upper crustal hydrothermal systems. *Scientific reports*, 9(1):9209, 2019.
- [31] S. Masoch, M. Fondriest, N. Preto, M. Secco, and G. Di Toro. Seismic cycle recorded in cockade-bearing faults (Col de Teghime, Alpine Corsica). *Journal of Structural Geology*, 129:103889, 2019.
- [32] M. Pec, H. Stünitz, R. Heilbronner, M. Drury, and C. de Capitani. Origin of pseudotachylites in slow creep experiments. *Earth Planet. Sci. Lett.*, 355:299–310, 2012.
- [33] Kevin M Brown and Yuri Fialko. 'Melt welt' mechanism of extreme weakening of gabbro at seismic slip rates. *Nature*, 488(7413):638, 2012.
- [34] G. Di Toro, D. L. Goldsby, and T. E. Tullis. Friction falls towards zero in quartz rock as slip velocity approaches seismic rates. *Nature*, 427:436–439, 2004.
- [35] Nir Z Badt, Terry E Tullis, Greg Hirth, and David L Goldsby. Thermal pressurization weakening in laboratory experiments. *J. Geophys. Res.*, 125(5):e2019JB018872, 2020.
- [36] Jianye Chen, Berend A Verberne, and Christopher J Spiers. Effects of healing on the seismogenic potential of carbonate fault rocks: Experiments on samples from the Longmenshan Fault, Sichuan, China. J. Geophys. Res., 120(8):5479-5506, 2015.
- [37] André R Niemeijer and Cristiano Collettini. Frictional properties of a low-angle normal fault under in situ conditions: thermally-activated velocity weakening. Pure Appl. Geophys., 171(10):2641–2664, 2014.
- [38] ME French, FM Chester, and JS Chester. Micromechanisms of creep in clay-rich gouge from the Central Deforming Zone of the San Andreas Fault. J. Geophys. Res., 120(2):827–849, 2015.

- [39] B A Verberne, A R Niemeijer, J HP De Bresser, and C J Spiers. Mechanical behavior and microstructure of simulated calcite fault gouge sheared at 20-600°C: Implications for natural faults in limestones. J. Geophys. Res., 120(12):8169–8196, 2015.
- [40] Keishi Okazaki and Ikuo Katayama. Slow stick slip of antigorite serpentinite under hydrothermal conditions as a possible mechanism for slow earthquakes. *Geophys. Res. Lett.*, 42(4):1099–1104, 2015.

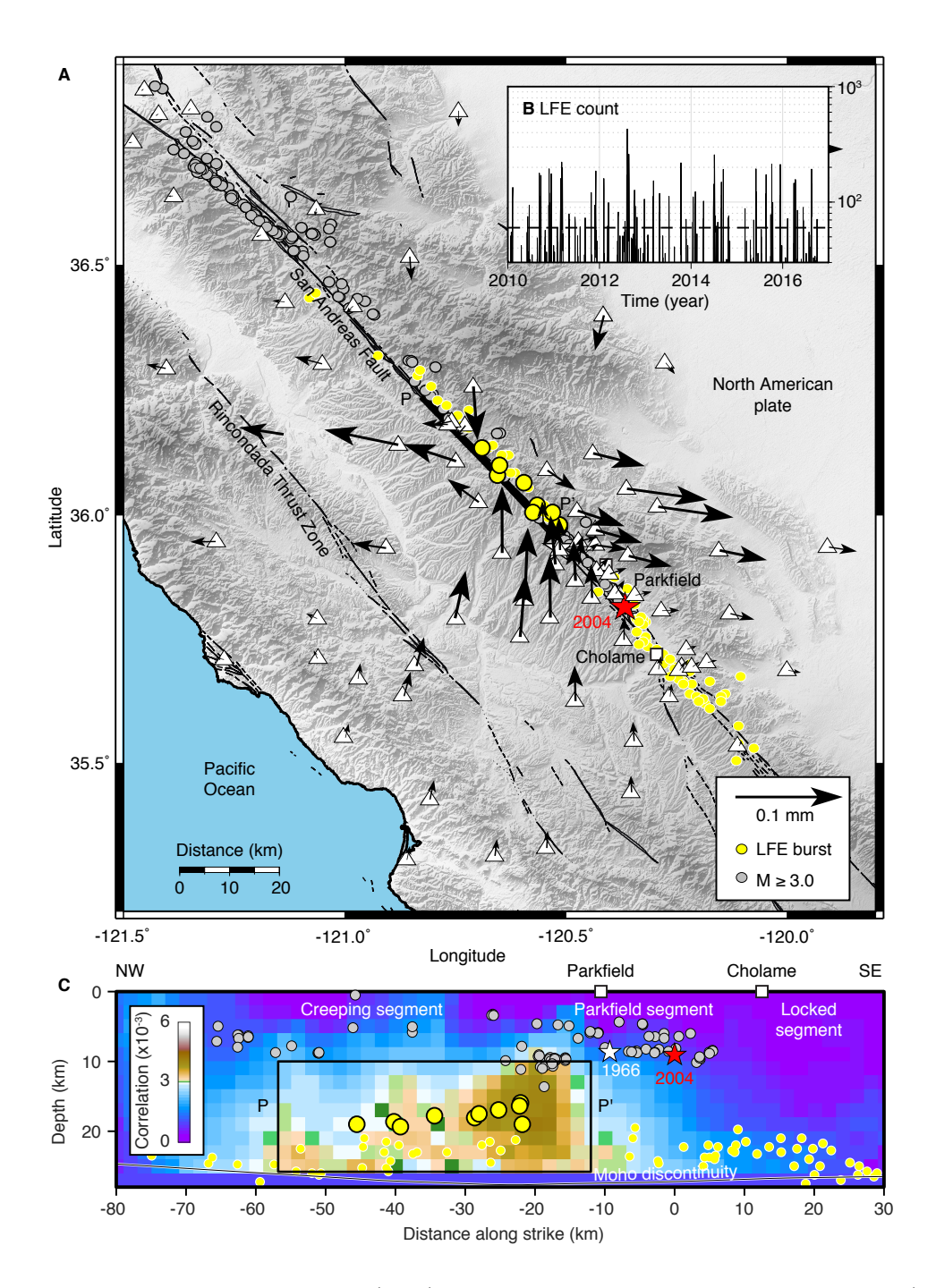


Figure 1: Deep low-frequency earthquakes (LFE) and slow slip along the San Andreas Fault. a) LFE [9] (yellow circles) and Mw≥3 seismicity from the NCEDC catalogue (gray circles) for the period 2004-2017. The 10 LFE families above 20 km depth are marked with a black contour. The Mw 6.0 Parkfield earthquakes of 1966 and 2004 are marked by the white and red stars, respectively. The displacements (black vectors) at GPS sites (white triangles) are due to a simulated large slow-slip event of Mw 4.72, whose slip distribution is shown in Figure 3b. b) Temporal behavior of the shallowest ten LFE families northwest of Parkfield. c) Vertical cross-section along the San Andreas fault. The background color, associated with a correlation coefficient, indicates the likely location of a slow-slip event driving the shallowest LFE [11].

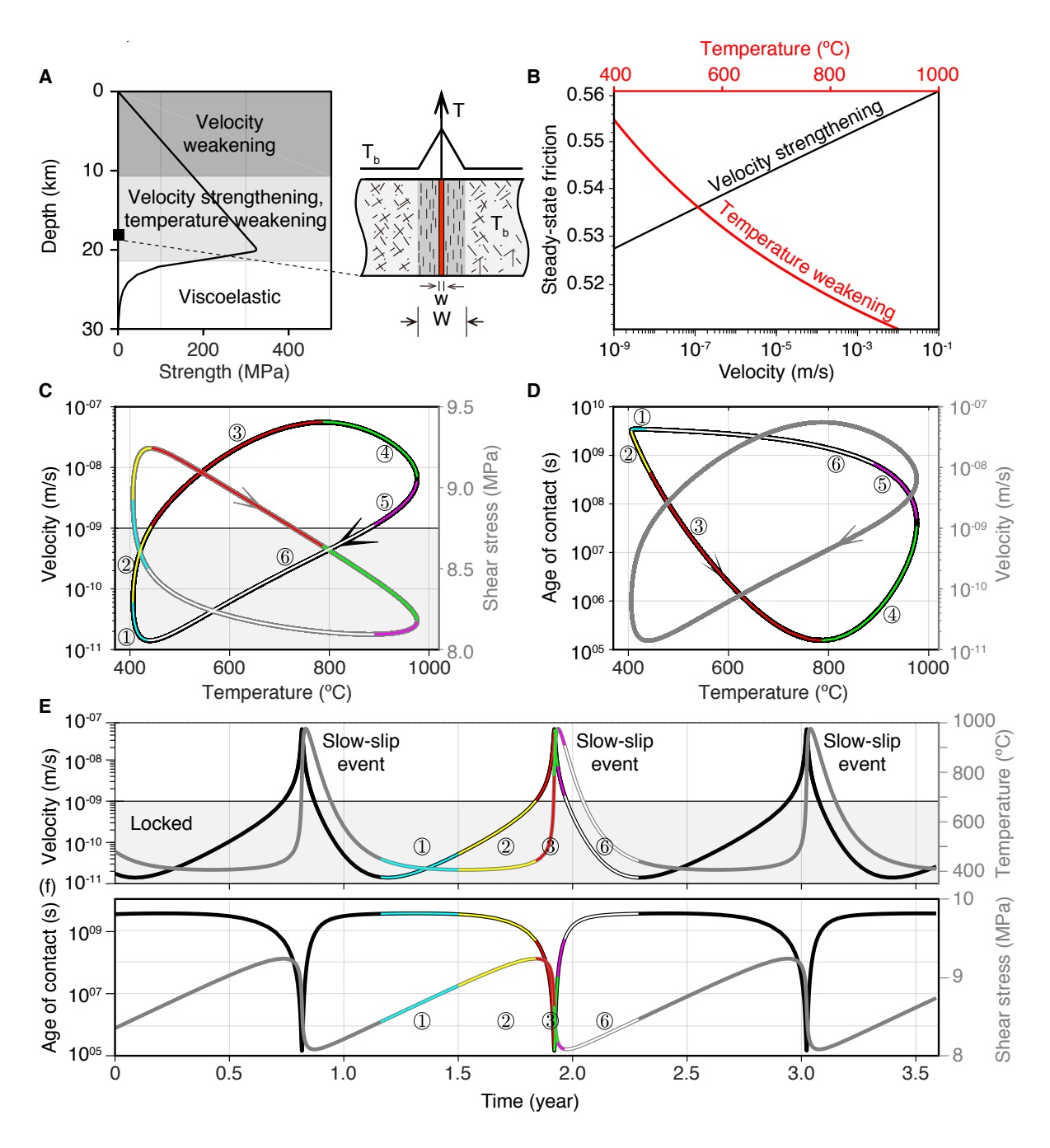


Figure 2: Thermal instabilities in a spring-slider assembly. A) Schematic strength profile showing the velocity-weakening shallow crust above a velocity-strengthening mid-crust and a ductile lower crust. A velocity-strengthening, temperature-weakening fault patch undergoes shear heating in the active shear layer of thickness w. Temperature diffuses to the bath temperature T_b through a fault zone of thickness W. B) Dependence of steady-state friction on velocity and temperature. C) Repeat cycles among velocity and temperature, shear stress and temperature. D) Repeat cycles among age of contact and temperature, velocity and temperature. Different phases are indexed ordinally and labeled with different colors. E) Evolution of velocity and temperature during three slow-slip events. F) Corresponding evolution of the age of contact and shear stress.

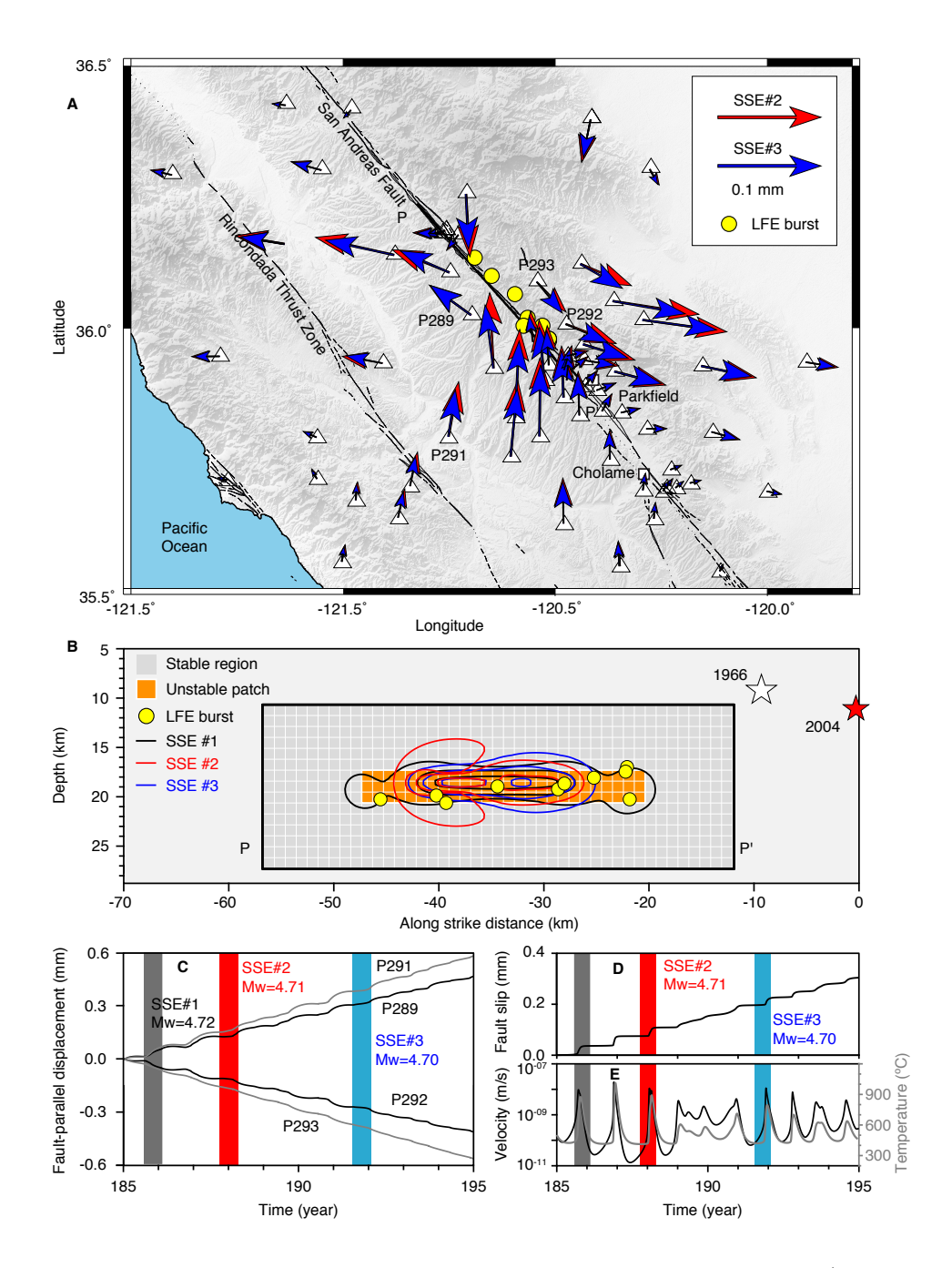


Figure 3: Numerical simulations of slow-slip events on the San Andreas fault. A) The surface displacements produced by two slow-slip events representing partial ruptures of the unstable temperature-weakening area. B) Slip distribution of slow-slip events with contour lines for cumulative slip of 10, 20, and 30 mm. The black contour is for the slow-slip event of Mw 4.72 shown in Figure 1. C) Simulated fault-parallel surface displacements for GPS stations P292, P293, P289, and P291. D) Slip history at the center of the unstable patch. E) Temporal evolution of slip velocity (black) and temperature (gray) at the patch center.

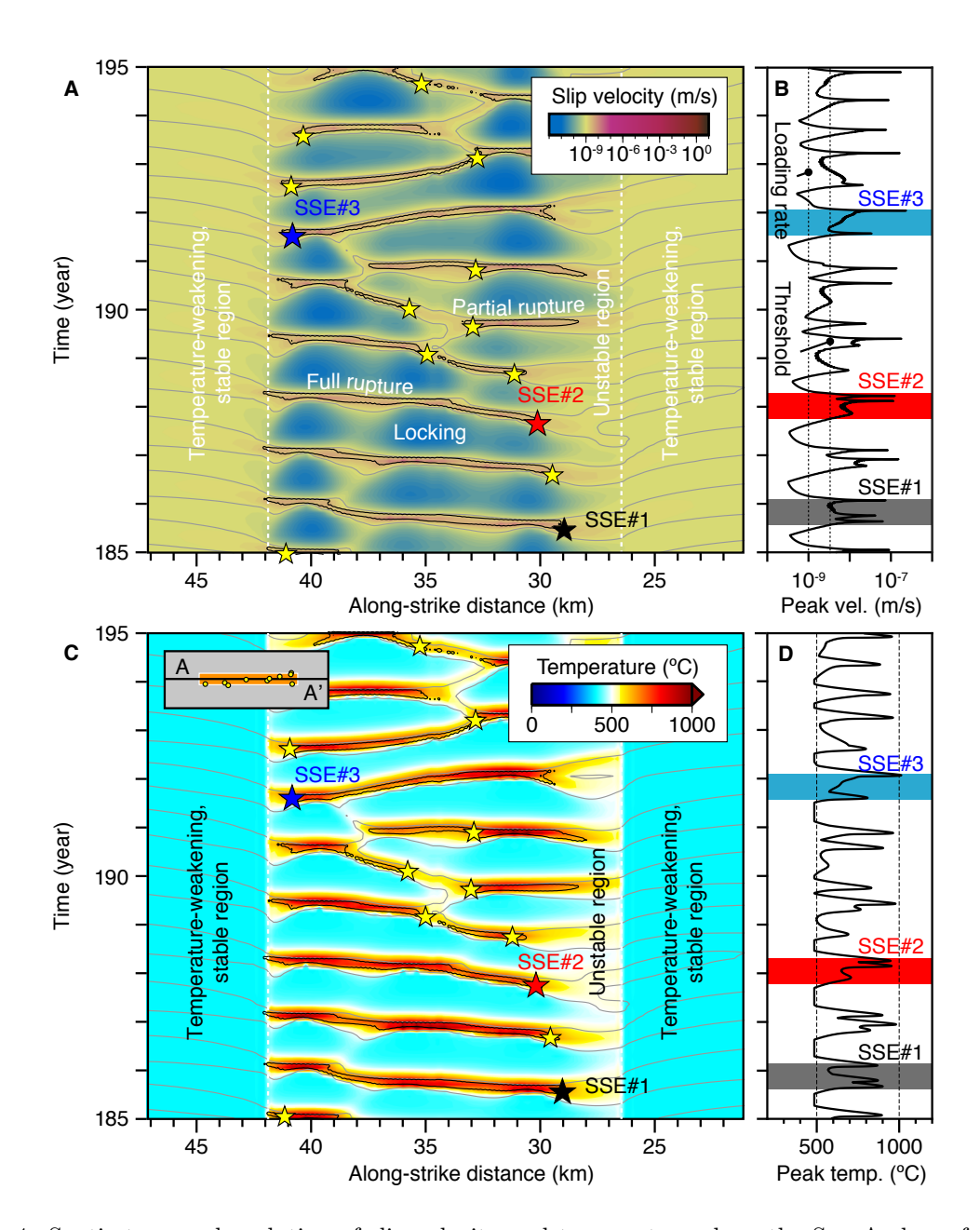


Figure 4: Spatio-temporal evolution of slip velocity and temperature along the San Andreas fault. A) Horizontal velocity profile A-A' at 17 km depth showing a complex sequence of slow-slip events. The inset locates the profile. Light gray and dark lines indicate contour of velocity of 1 and 3 nm/s, respectively. Dark profiles indicate velocity above 3 nm/s. B) Evolution of maximum velocity anywhere on the fault. C) Evolution of temperature on profile A-A'. The contours are same as in a). d) Evolution of maximum temperature anywhere on the fault.

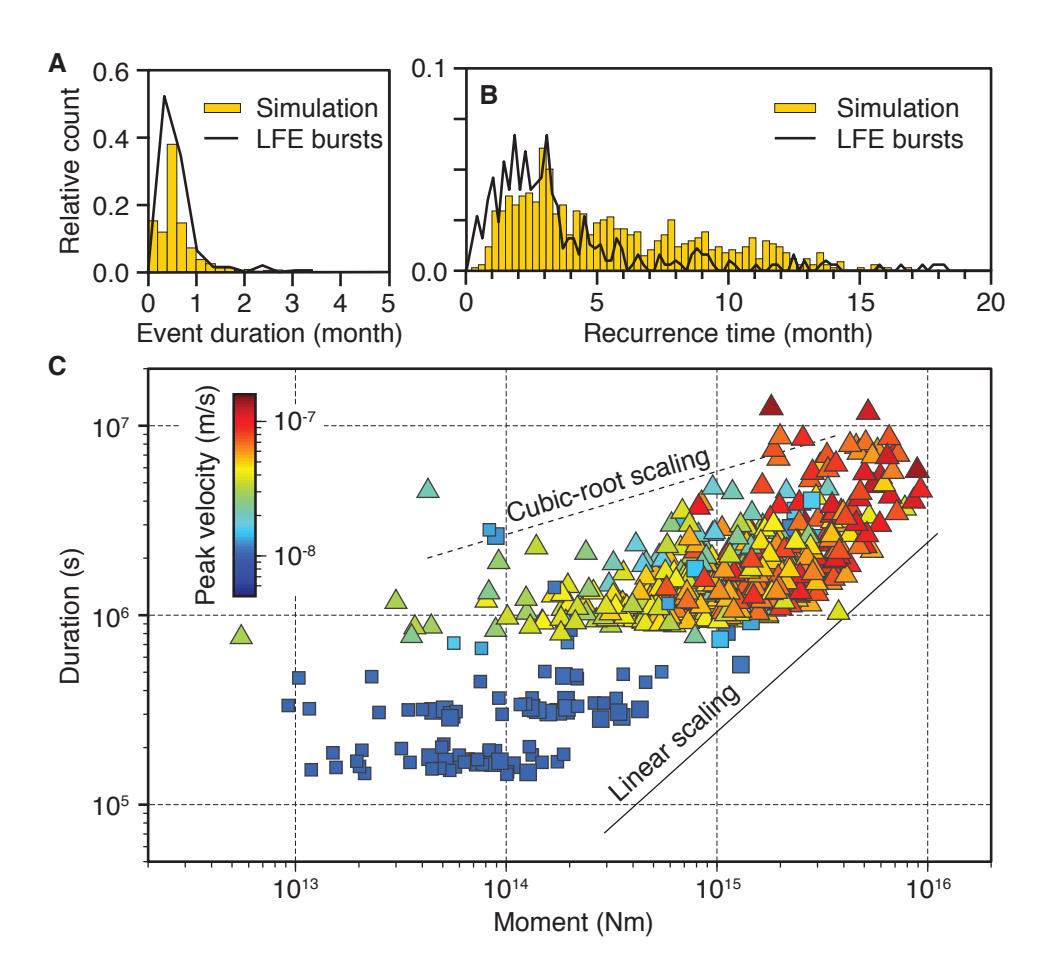


Figure 5: Recurrence pattern of Parkfield LFE and simulated events. A) Histograms of recurrence times for simulated slow-slip events (bars) and for the 10 shallow LFE sources (thick profile). B) Histograms of event duration for slimulated slow-slip events and the same LFE sources. C) Moment-duration scaling for the catalogue of simulated slow-slip events. The scaling for linear (solid line) and cubic (dashed line) relationships is shown for reference. Two clusters of events can be determined based on the peak velocity, below (squares) or above (triangles) $V_{\rm peak} = 1.6 \times 10^{-8} \, {\rm m/s}$, associated with different moment/duration scaling.

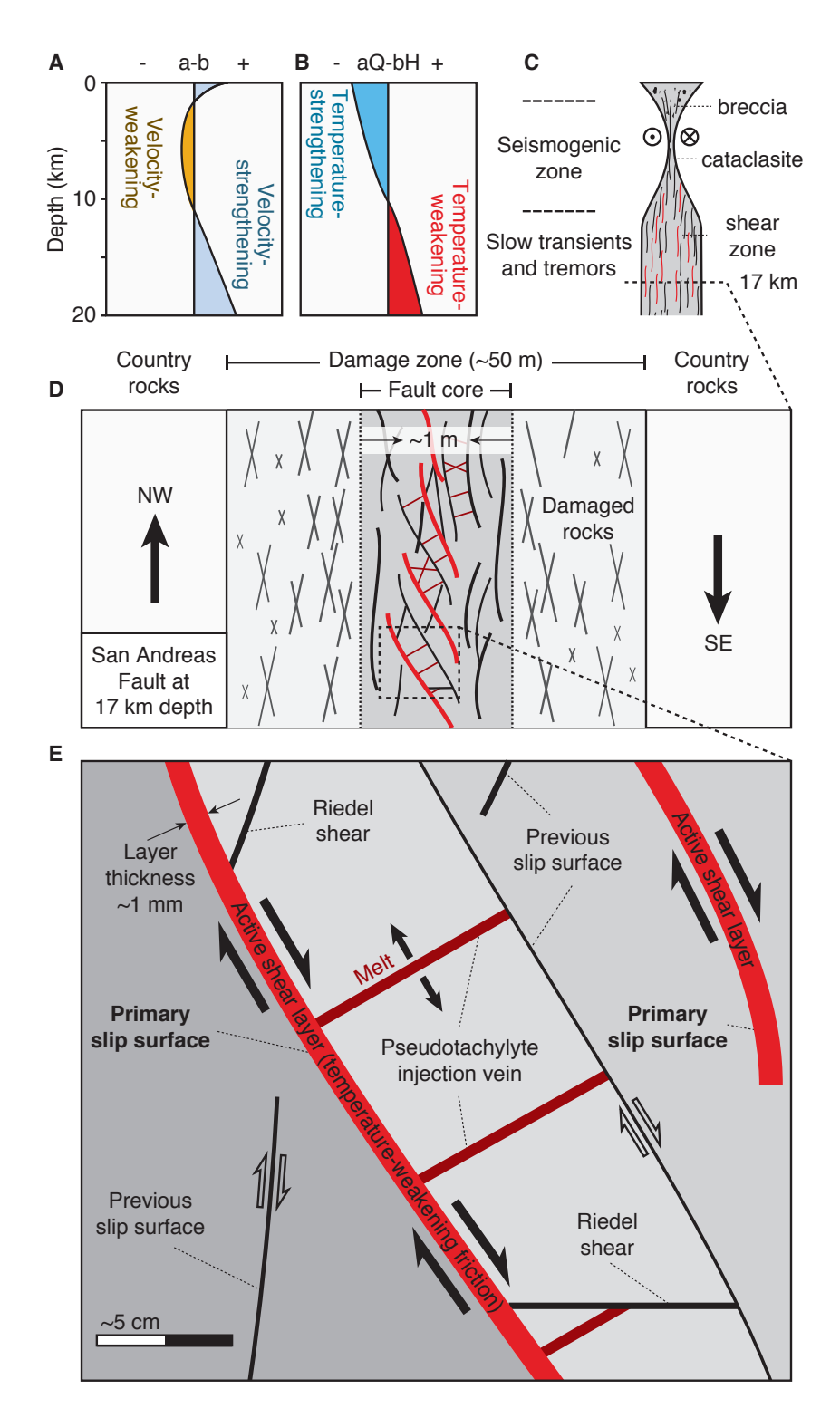


Figure 6: Schematic of mechanical properties of the San Andreas Fault in the brittle regime. A) Depth-dependence of the steady-state frictional properties a-b that control the velocity dependence. B) Depth-dependence of the steady-state frictional properties aQ-bH that control the temperature dependence. Thermal instabilities may occur in a temperature-weakening domain, depending on stability conditions. C) Fault fabric at depth and seismic cycle behavior. D) Horizontal section of a shear zone at the root of the San Andreas fault with multi-stranded slip surfaces. E) Details of the fault core with primary slip surfaces associated with shear heating and pseudotachylyte injection veins resulting from partial melting during slow slip events.